

Stress Relaxation above and below the Jamming Transition

Kuniyasu Saitoh^{1,*}, Takahiro Hatano², Atsushi Ikeda^{3,4}, and Brian P. Tighe⁵

¹Research Alliance Center for Mathematical Sciences, Tohoku University, 2-1-1 Katahira, Aoba-ku, Sendai 980-8577, Japan

²Department of Earth and Space Science, Osaka University, 560-0043 Osaka, Japan

³Graduate School of Arts and Sciences, University of Tokyo, Tokyo 3-8-1, Japan

⁴Research Center for Complex Systems Biology, Universal Biology Institute, University of Tokyo, Komaba, Tokyo 153-8902, Japan

⁵Delft University of Technology, Process & Energy Laboratory, Leeghwaterstraat 39, 2628 CB Delft, Netherlands



(Received 22 September 2019; accepted 26 February 2020; published 16 March 2020)

We numerically investigate stress relaxation in soft athermal disks to reveal critical slowing down when the system approaches the jamming point. The exponents describing the divergence of the relaxation time differ dramatically depending on whether the transition is approached from the jammed or unjammed phase. This contrasts sharply with conventional dynamic critical scaling scenarios, where a single exponent characterizes both sides. We explain this surprising difference in terms of the vibrational density of states, which is a key ingredient of linear viscoelastic theory. The vibrational density of states exhibits an extra slow mode that emerges below jamming, which we utilize to demonstrate the anomalous exponent below jamming.

DOI: [10.1103/PhysRevLett.124.118001](https://doi.org/10.1103/PhysRevLett.124.118001)

Amorphous materials such as suspensions, emulsions, foams, and granular materials are important in engineering science, and a better understanding of their rheology is of central importance in many manufacturing processes [1]. Although the rheophysics of amorphous materials has a long history, a predictive description of their elastovisco-plastic response remains challenging [2]. Recently, physicists have focused on steady shear flow near the jamming transition at the packing fraction ϕ_J [3–14]. Sufficiently close to jamming ($\Delta\phi \equiv \phi - \phi_J \rightarrow \pm 0$), rheological flow curves (stress-strain rate relations) can be collapsed to master curves [3], reminiscent of critical scaling functions near a second order phase transition [15]. Critical scaling implies the existence of a diverging timescale, $t_{sf} \sim |\Delta\phi|^{-\alpha}$. While details of the jamming scaling scenario remain controversial, there is general agreement that the exponent α is the same on either side of the transition, with estimates for its value ranging from 2 to 3 [16].

Steady shear flow is not the only way to probe timescales near jamming—viscoelastic tests can also be used. Viscosities measured via stress relaxation or oscillatory shear need not match the steady state viscosity, though in practice they are often comparable [1]. Unlike steady flow, numerical studies of viscoelasticity typically apply perturbations to an isotropic reference state. This is an important distinction, because there is evidence that (nearly) jammed states encode their loading history in their vibrational spectrum. Lerner *et al.* related the divergence of t_{sf} to this self-organization under steady shear [17], and recently Ikeda *et al.* identified similar effects under isotropic compression [18]. However, it remains unclear what happens when a system is prepared isotropically and then subjected to a transverse stress increment, i.e., shear.

Above jamming, small amplitude oscillatory shear and stress relaxation tests in $D = 2$ dimensions reveal a diverging relaxation time $t_+^* \sim \Delta\phi^{-\nu_+}$ with $\nu_+ = 1$ [19–21]—the viscoelastic relaxation time also diverges, albeit more slowly than t_{sf} . This result is consistent with theoretical predictions for both $D = 2$ and 3, which relate t_+^* to a broadening distribution of overdamped eigenmodes near ϕ_J [22]. Three-dimensional stress relaxation tests below jamming also reveal a diverging timescale, $t_-^* \sim |\Delta\phi|^{-\nu_-}$ [23]. However, the exponent $\nu_- \approx 3.3$ is much larger than unity, reminiscent of the exponent α for steady flow. The large difference between ν_+ and ν_- represents a surprising departure from conventional dynamic critical scaling, where a single exponent describes the divergence on both sides of the transition [15]. The conventional scenario is in fact observed in closely related systems of overdamped spring networks, with $\nu_+ = \nu_- = 1$ [24]. Hence, from this perspective ν_- is the anomalous exponent. Resolving this discrepancy and understanding its origin represent an important challenge in jamming and rheology.

In this Letter, we use molecular dynamics simulations of 2D stress relaxation tests to present the first simultaneous measurements of ν_+ and ν_- . We verify the large difference between the two exponents, eliminating the possibility that their difference was spurious or due to different measurement techniques. We further establish qualitative similarities between viscoelastic relaxation and steady state rheology below jamming, including the anomalously large value of ν_- . We relate this difference to the same self-organization process identified previously in steady flow and isotropic cooling.

Numerical methods.—We perform simulations of 50:50 binary mixtures of N disks with diameter ratio 1.4:1, a

standard model in the jamming literature [25,26]. Initial conditions are prepared in a $L \times L$ square periodic box [27] at a controlled area fraction ϕ near the jamming point $\phi_J \simeq 0.8433$. The force between the disks, i and j , in contact is modeled as $\mathbf{f}_{ij}^{\text{el}} = k\xi_{ij}\mathbf{n}_{ij}$, where k is the stiffness and $\mathbf{n}_{ij} \equiv \mathbf{r}_{ij}/|\mathbf{r}_{ij}|$ is the normal unit vector, with $\mathbf{r}_{ij} \equiv \mathbf{r}_i - \mathbf{r}_j$ the relative position vector. The force is linear in the overlap $\xi_{ij} \equiv R_i + R_j - |\mathbf{r}_{ij}| > 0$, where R_i (R_j) is the radius of the disk i (j). The motion of the disk i is described by overdamped dynamics [3,4,7,23]; i.e., $k\sum_j \xi_{ij}\mathbf{n}_{ij} + \eta\dot{\mathbf{r}}_i = \mathbf{0}$, where η is introduced as the damping coefficient. In this model, the stiffness and damping coefficient determine a timescale $t_0 \equiv \eta/k$.

Relaxation tests.—To study viscoelastic properties of a packing, we apply a small strain step γ to the system, where every disk's position (x_i, y_i) is replaced with $(x_i + \gamma y_i, y_i)$ under the Lees-Edwards boundary conditions [23]. Figure 1(a) shows a snapshot of the anisotropic force chains (solid lines) that develop immediately after the simple shear deformation. The affine displacements $\mathbf{u}_i^{\text{affine}} = (\gamma y_i, 0)$ generate force imbalances, and for $t > 0$ the particles are allowed to relax to a new mechanical equilibrium while γ is held fixed via the Lees-Edwards boundary conditions. As in Fig. 1(b), we observe complex nonaffine displacements of the disks, $\delta\mathbf{u}_i = \mathbf{u}_i - \mathbf{u}_i^{\text{affine}}$, during the relaxation. After relaxation the initial force

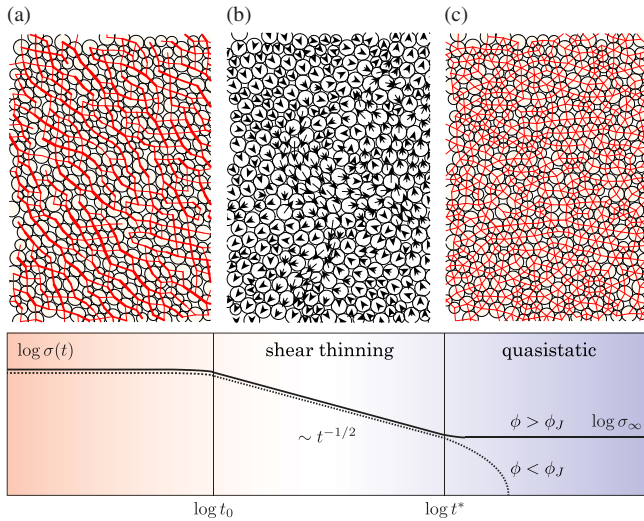


FIG. 1. (a) Anisotropic force chains (solid lines) immediately after applying a step strain $\gamma = 10^{-2}$ to the packing with $\phi = 0.9$, where the line width is proportional to the strength of elastic force between the disks (circles) in contact. (b) Nonaffine displacements $\delta\mathbf{u}_i$ (arrows) during the relaxation and (c) force chains after the relaxation. The lower panel is a sketch of *stress relaxation* $\sigma(t)$, where the solid and dotted lines are the shear stress above and below the jamming transition, respectively. The power-law relaxation $\sigma(t) \sim t^{-1/2}$ is observed in shear thinning regime $t_0 < t < t^*$. In quasistatic limit $t > t^*$, the shear stress is finite ($\sigma_\infty > 0$) above jamming, while it drops to zero below jamming.

chains are significantly weakened [Fig. 1(c)] and the shear stress has been reduced. Shear stress is calculated as $\sigma(t) = -L^{-2} \sum_{i>j} f_{ijx}^{\text{el}}(t)r_{ijy}(t)$, where $f_{ijx}^{\text{el}}(t)$ and $r_{ijy}(t)$ are the x and y components of the elastic force and relative position, respectively. We neglect infinitesimal kinetic contributions to the stress and subtract the *prestress* (the shear stress in prepared packing) from numerical data to reduce noise.

If the strain step is sufficiently small, $\gamma \ll 1$, the shear stress is described by linear viscoelasticity [1],

$$\sigma(t) = \int_{-\infty}^t G(t-t')\dot{\gamma}(t')dt' = \gamma G(t), \quad (1)$$

where $\dot{\gamma}(t) = \gamma\delta(t)$ is the imposed shear rate and $G(t)$ is the stress relaxation modulus. Figure 2 displays our numerical results of scaled shear modulus $G(t)/G(0)$, where the area fraction ϕ increases across the jamming point ϕ_J (as indicated by the arrow). We observe instantaneous responses on a short timescale $t < t_0$ regardless of the area fraction. Below jamming ($\phi < \phi_J$), the shear stress ultimately decays to zero, while it asymptotically decreases to a finite *remnant stress* $\sigma_\infty = \gamma G_\infty$ above jamming ($\phi > \phi_J$). As the system approaches the jamming transition, we find power-law decay $G(t) \sim t^{-1/2}$ in the intermediate timescale $t_0 < t < t^*$, where the relaxation time t^* strongly depends on the proximity to jamming. From these observations, we divide the time development of shear modulus into three different regimes: (i) instantaneous response $G(t) \sim \text{const}$, (ii) shear thinning $G(t) \sim t^{-1/2}$, and (iii) quasistatic limit $G(t) \sim 0$ for $\phi < \phi_J$ and $G(t) \sim G_\infty$ for $\phi > \phi_J$ [22].

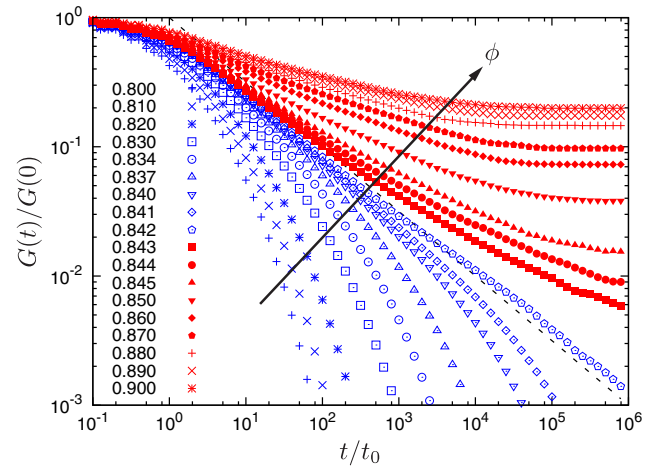


FIG. 2. Double logarithmic plots of the scaled shear modulus $G(t)/G(0)$ and scaled time t/t_0 , where the dotted line represents the power-law decay $G(t) \sim t^{-1/2}$. The area fraction ϕ increases as indicated by the arrow and listed in the legend, where the (blue) open and (red) closed symbols represent the data below ($\phi < \phi_J$) and above jamming ($\phi > \phi_J$), respectively. Here, $\gamma = 10^{-2}$ is applied to $N = 131\,072$ disks.

Critical divergence of the relaxation time.—To estimate the relaxation time t^* , we collapse the data of the shear modulus. Prior work has investigated the dependence of stress response on the strain step size. Above jamming, Boschan *et al.* [20] found that linear response holds, so long as the strain step is smaller than the excess packing fraction $\Delta\phi$. Below jamming, studies by Hatano indicate that $G(t)$ is insensitive to the step size for values as large as $\gamma = 0.05$ [23]. We have verified these results in our own simulations, and choose $\gamma = 10^{-4}$ above jamming and $\gamma = 10^{-2}$ below. Figure 3 plots $G(t)$ against time, where they are scaled by $|\Delta\phi|^{\lambda_{\pm}}$ and $|\Delta\phi|^{\nu_{\pm}}$, respectively. The data above jamming (closed symbols) are well collapsed by the exponents, $\lambda_+ = 0.5$ and $\nu_+ = 1.0$, implying emergence of the static shear modulus $G_{\infty} \propto \Delta\phi^{1/2}$ and divergence of the relaxation time $t^* \sim \Delta\phi^{-1}$. These results are consistent with prior numerical measurements [19–21] and theoretical predictions [22]. On the other hand, we find excellent data collapse for data below jamming (open symbols) using $\lambda_- = 1.25$ and $\nu_- = 2.7$. Note that the scaling relation $\lambda_{\pm}/\nu_{\pm} \simeq 1/2$ is satisfied both above and below jamming [see Supplemental Material (SM) [28]]. Therefore, the relaxation time scales differently on either side of jamming:

$$t^* \sim \begin{cases} \Delta\phi^{-1} & (\phi > \phi_J) \\ |\Delta\phi|^{-2.7} & (\phi < \phi_J). \end{cases} \quad (2)$$

Linear viscoelastic theory.—We now rationalize the two different scaling relations of Eq. (2) using viscoelastic theory [22] and numerical measurements of the relaxation spectrum. To begin, it is useful to note certain properties of $i\omega G^*(\omega)$, the Fourier transform of $G(t)$. Here $G^* = G' + iG''$ is known as the complex shear modulus, while G' and G'' are the storage and loss moduli, respectively. Because

$G(t)$ is a real-valued function, G' (G'') must be even (odd) in ω . Assuming G^* is analytic and taking the limit $\omega \rightarrow 0$, it follows that $G' - G_{\infty} \sim \omega^2$ and $G'' \sim \omega$. [We recall that $G_{\infty} \equiv G'(0)$ is zero in a fluid and finite in a solid.] The relaxation time is the scale where these elastic and viscous contributions to the stress balance:

$$t^* = \lim_{\omega \rightarrow 0} \frac{G' - G_{\infty}}{\omega G''}. \quad (3)$$

We will use Eq. (3) to evaluate t^* within the harmonic approximation by expanding about a reference state. We choose the state at $t \rightarrow \infty$, as determined from numerics. Above jamming, one could also choose the initial condition as a reference state because, for any finite sized system, the strain step can always be taken small enough that no contacts are made or broken. Below jamming, however, the initial condition contains only “kissing” contacts and the initial, affine shear step necessarily alters the contact network, which violates the harmonic approximation. At long times, however, the contact network assumes its final topology (see SM [28]) and the approximation can be applied. Given a reference configuration, the complex shear modulus can be calculated from

$$G^*(\omega) = \{G_a + i\eta\omega\} - L^{-D} \langle \tilde{\mathbf{u}}(\omega) | [\mathcal{K} - i\eta\omega \mathbf{1}] | \tilde{\mathbf{u}}(\omega) \rangle. \quad (4)$$

The ket $|\tilde{\mathbf{u}}(\omega)\rangle$ contains the Fourier transform of the particles’ displacements from their reference positions, and \mathcal{K} is the Hessian matrix. The term G_a is the affine shear modulus, which remains finite at jamming. The second term on the right-hand side of Eq. (4) is the nonaffine contribution to the modulus. A derivation of Eq. (4) is given in the SM [28].

Next we introduce the eigenfrequencies ω_n and eigenvectors $|n\rangle$ ($n = 1, \dots, 2N$) of the Hessian \mathcal{K} . By expressing the $2N$ -dimensional vector $|\tilde{\mathbf{u}}(\omega)\rangle$ as a linear combination of the eigenvectors and taking the limit of vanishing frequency, Eq. (3) becomes

$$t^* \sim \frac{\sum_n \Xi_n^2 / \omega_n^6}{\sum_n \Xi_n^2 / \omega_n^4}. \quad (5)$$

Here $|\Xi\rangle$ is the net force imbalance per unit affine shear and $\Xi_n \equiv |\langle n | \Xi \rangle|$ is its projection onto the n th mode. Ξ_n is a measure of the mode’s coupling to shear.

Vibrational density of states (VDOS).—In order to analyze the scaling of Eq. (5) near jamming, it is necessary to quantify the spectrum of eigenfrequencies $\{\omega_n\}$. We therefore introduce $D(\omega_n)$, the vibrational density of states. As shown previously [29] and in the SM [28], the VDOS above jamming exhibits a plateau, $D(\omega_n) \sim \text{const}$, extending to a characteristic scale ω^* that vanishes at unjamming [30]. We find a similar scenario holds below jamming: Fig. 4(a) reveals the same plateau over a range $\omega^* < \omega_n < t_0^{-1}$ (dotted

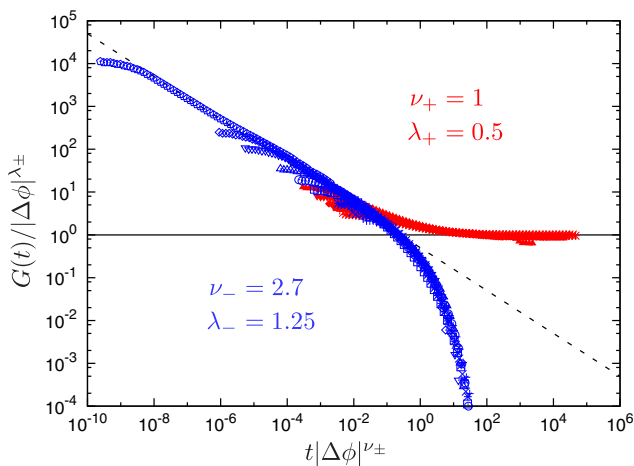


FIG. 3. Data collapses of the stress relaxation modulus $G(t)$, where the dotted line and symbols are as in Fig. 2. The horizontal solid line indicates the static shear modulus $G_{\infty} \sim |\Delta\phi|^{\lambda_{\pm}}$. See the text for the exponents, ν_{\pm} and λ_{\pm} .

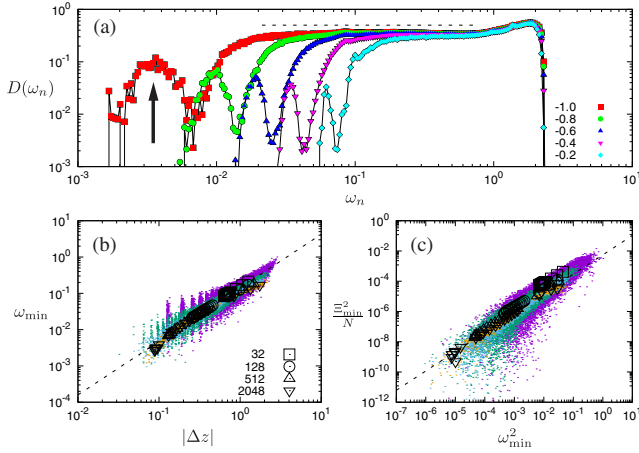


FIG. 4. (a) Double logarithmic plots of the averaged VDOS for $N = 2048$ disks below jamming, where $\gamma = 10^{-2}$ is applied to the systems and $\log_{10} |\Delta z|$ increases as listed in the legend. The dotted line and arrow indicate the plateau ($\omega^* < \omega_n$) and extra mode ω_{\min} for $|\Delta z| = 10^{-1}$, respectively. (b),(c) Scatter plots of (b) ω_{\min} and $|\Delta z|$ and (c) Ξ_{\min}^2/N and ω_{\min}^2 . The open symbols are averages over each area fraction ϕ , where the system size N increases as listed in the legend of (b). The dotted lines indicate (b) $\omega_{\min} \sim |\Delta z|^{1.47}$ and (c) $\Xi_{\min}^2 \sim N\omega_{\min}^{2.56}$.

line), with $\omega^* \sim |\Delta z|^{1.3}$ controlled by the excess coordination number $\Delta z \equiv z - z_c$ ($z_c = 4$ in two dimensions) [31].

In addition, as indicated by the arrow in Fig. 4(a), there is a narrow band of slow modes below ω^* . (Note that packings below jamming also contain a number of *floppy modes* with $\omega_n = 0$, which are not visible in a log-log plot.) The finite frequency band is centered on a peak value ω_{\min} that also goes to zero as the system approaches ϕ_j from below. The finite width of this band is the result of averaging over 10^3 different configurations—in fact, as we show in the SM [28], each packing contributes a single mode near ω_{\min} , well separated from the modes at $\omega \gtrsim \omega^*$. Such a “special mode” below jamming was previously observed by Lerner *et al.* in steady shear flow [17] and by Ikeda *et al.* [18] in isotropic cooling. At the same time, randomly cut under-coordinated spring networks have no such special mode, although their VDOS is otherwise similar [22,32,33]. These results suggest that loading trains the system to “know about” a particular direction in stress-space, by (self-)organizing to support the load. This, in turn, is encoded in the special mode. A related process above jamming leads to the jump in the bulk modulus [34–36]. Our systems are prepared via an isotropic process and then subjected to shear, so (unlike prior work) the stress increment is transverse to the preparatory load. It is therefore not self-evident if or how the special mode should influence the dynamic viscosity.

Scaling analysis.—The exponent $\nu_+ = 1$ characterizing relaxation above jamming was derived in Ref. [22], so we focus here on the case below jamming. In order to perform scaling analysis, we numerically measure ω_{\min} and the

coupling strengths. Figure 4(b) displays scatter plots of ω_{\min} and $|\Delta z|$, where each dot is the result of one configuration of the disks. Each symbol is the average of ω_{\min} over packings with the same area fraction ϕ . The mode frequency scales as $\omega_{\min} \sim |\Delta z|^{1.47}$ (dotted line), independent of the system size N (colors and symbols).

Excluding the special mode, the coupling strengths scale as $\Xi_n^2 \sim \omega_n^2$, independent of N . This relation, which implies that floppy modes have no shear coupling [$\Xi_n(\omega_n = 0) = 0$], has been validated numerically for unstressed systems above jamming [37]. In the SM [28] we motivate it theoretically and confirm that it holds below jamming as well. In sharp contrast, Fig. 4(c) shows that coupling strengths for the special mode collapse when plotting Ξ_{\min}^2/N versus ω_{\min}^2 for different sizes (colors and symbols). This implies $\Xi_{\min}^2 \sim N\omega_{\min}^{2.56}$ (dotted line). Note, in particular, that Ξ_{\min}^2 is extensive; i.e., it couples to shear differently, and more strongly, than other modes. This strong coupling to shear is surprising, in the sense that the system was prepared isotropically. Evidently, the reorganization triggered by a small shear step is sufficient to develop the special mode—which does not occur above jamming. We attribute this difference to the fact that any strain step can make or break contacts, whereas finite size systems above jamming can be probed without inducing rearrangements [19,38–40].

Because the special mode is the softest nonfloppy mode in the system and couples extensively to shear, it dominates each of the sums on the right-hand side of Eq. (5), with all other modes contributing subdominantly. One finds

$$t^* \sim \omega_{\min}^{-2} \sim |\Delta z|^{-2.94}, \quad (6)$$

which agrees with Eq. (2) because $|\Delta z| \sim |\Delta\phi|$ [28,41]. Hence, while relaxation above jamming is controlled by ω^* [22], below jamming it is set by ω_{\min} . This explains the difference in scaling of the relaxation time on either side of the transition.

Summary and outlook.—In this study, we numerically studied stress relaxation in soft athermal disks. The relaxation time diverges when the system approaches the jamming point—but, unusually, the critical exponent depends on the direction of approach [Eq. (2)]. We calculated the VDOS and found its plateau above the characteristic scale ω^* . In contrast, the VDOS below jamming has a delta peak at a special mode $\omega_{\min} (< \omega^*)$. Using scaling analysis, we showed that ω_{\min} controls long time relaxation below jamming by setting the value of ν_- . As the same approach correctly predicts ν_+ above jamming, as well [22], we have unified the theoretical description of relaxation on either side of jamming.

The results presented here were in 2D. Recent work by Olsson [6] has raised questions about the value of the scaling exponent for steady flow in 3D. Hence there is a need for a careful future study of t^* in 3D, building on the

work of Hatano [23]. As the special mode has also been demonstrated in 3D [17,18], we expect our approach to apply in that case as well. Other likely future directions include the role of the viscous force law [21] and, in particular, the role of inertia, where comparison with experiments [42] is important for industrial applications.

We thank E. Lerner, W. Kob, F. Radjai, K. Miyazaki, T. Kawasaki, H. Hayakawa, J. Boschan, and K. Baumgarten for fruitful discussions. This work was supported by KAKENHI Grants No. 16H04025 and No. 18K13464 from JSPS. Some computations were performed at the Yukawa Institute Computer Facility, Kyoto, Japan. B. P. T. acknowledges support from the Dutch Organization for Scientific Research (NWO).

*kuniyasu.saitoh.c6@tohoku.ac.jp

- [1] R. G. Larson, *The Structure and Rheology of Complex Fluids* (Oxford University Press, Inc., New York, 1999).
- [2] D. Bonn, M. M. Denn, L. Berthier, T. Divoux, and S. Manneville, *Rev. Mod. Phys.* **89**, 035005 (2017).
- [3] P. Olsson and S. Teitel, *Phys. Rev. Lett.* **99**, 178001 (2007).
- [4] P. Olsson and S. Teitel, *Phys. Rev. Lett.* **109**, 108001 (2012).
- [5] D. Vågberg, P. Olsson, and S. Teitel, *Phys. Rev. Lett.* **112**, 208303 (2014).
- [6] P. Olsson, *Phys. Rev. Lett.* **122**, 108003 (2019).
- [7] B. P. Tighe, E. Woldhuis, J. J. C. Remmers, W. van Saarloos, and M. van Hecke, *Phys. Rev. Lett.* **105**, 088303 (2010).
- [8] T. Hatano, *Prog. Theor. Phys. Suppl.* **184**, 143 (2010).
- [9] M. Otsuki and H. Hayakawa, *Phys. Rev. E* **80**, 011308 (2009).
- [10] K. N. Nordstrom, E. Verneuil, P. E. Arratia, A. Basu, Z. Zhang, A. G. Yodh, J. P. Gollub, and D. J. Durian, *Phys. Rev. Lett.* **105**, 175701 (2010).
- [11] B. Andreotti, J.-L. Barrat, and C. Heussinger, *Phys. Rev. Lett.* **109**, 105901 (2012).
- [12] A. Ikeda, L. Berthier, and P. Sollich, *Phys. Rev. Lett.* **109**, 018301 (2012).
- [13] T. Kawasaki, D. Coslovich, A. Ikeda, and L. Berthier, *Phys. Rev. E* **91**, 012203 (2015).
- [14] K. Saitoh and B. P. Tighe, *Phys. Rev. Lett.* **122**, 188001 (2019).
- [15] B. I. Halperin and P. C. Hohenberg, *Phys. Rev.* **177**, 952 (1969).
- [16] M. Trulsson, B. Andreotti, and P. Claudin, *Phys. Rev. Lett.* **109**, 118305 (2012).
- [17] E. Lerner, G. Düring, and M. Wyart, *Proc. Natl. Acad. Sci. U.S.A.* **109**, 4798 (2012).
- [18] A. Ikeda, T. Kawasaki, L. Berthier, K. Saitoh, and T. Hatano, *Phys. Rev. Lett.* **124**, 058001 (2020).
- [19] J. Boschan, D. Vågberg, E. Somfai, and B. P. Tighe, *Soft Matter* **12**, 5450 (2016).
- [20] J. Boschan, S. A. Vasudevan, P. E. Boukany, E. Somfai, and B. P. Tighe, *Soft Matter* **13**, 6870 (2017).
- [21] K. Baumgarten and B. P. Tighe, *Soft Matter* **13**, 8368 (2017).
- [22] B. P. Tighe, *Phys. Rev. Lett.* **107**, 158303 (2011).
- [23] T. Hatano, *Phys. Rev. E* **79**, 050301(R) (2009).
- [24] B. P. Tighe, *Phys. Rev. Lett.* **109**, 168303 (2012).
- [25] C. S. O’Hern, L. E. Silbert, A. J. Liu, and S. R. Nagel, *Phys. Rev. E* **68**, 011306 (2003).
- [26] D. J. Koeze, D. Vågberg, B. B. Tjoa, and B. P. Tighe, *Eur. Phys. Lett.* **113**, 54001 (2016).
- [27] E. Bitzek, P. Koskinen, F. Gähler, M. Moseler, and P. Gumbsch, *Phys. Rev. Lett.* **97**, 170201 (2006).
- [28] See Supplemental Material at <http://link.aps.org/supplemental/10.1103/PhysRevLett.124.118001> for the scaling relation, viscoelastic theory, and additional data.
- [29] L. E. Silbert, A. J. Liu, and S. R. Nagel, *Phys. Rev. Lett.* **95**, 098301 (2005).
- [30] M. van Hecke, *J. Phys. Condens. Matter* **22**, 033101 (2010).
- [31] The coordination number z is measured after fully relaxing the system and removing floating disks (with $z = 0$).
- [32] G. Düring, E. Lerner, and M. Wyart, *Soft Matter* **9**, 146 (2013).
- [33] M. G. Yucht, M. Sheinman, and C. P. Broedersz, *Soft Matter* **9**, 7000 (2013).
- [34] M. Wyart, *Ann. Phys. Fr.* **30**, 1 (2005).
- [35] M. Merkel, K. Baumgarten, B. P. Tighe, and M. L. Manning, *Proc. Natl. Acad. Sci. U.S.A.* **116**, 6560 (2019).
- [36] D. B. Liarte, X. Mao, O. Stenull, and T. C. Lubensky, *Phys. Rev. Lett.* **122**, 128006 (2019).
- [37] H. Mizuno, K. Saitoh, and L. E. Silbert, *Phys. Rev. E* **93**, 062905 (2016).
- [38] J. Boschan, S. Luding, and B. P. Tighe, *Granular Matter* **21**, 58 (2019).
- [39] M. S. van Deen, J. Simon, Z. Zeravcic, S. Dagois-Bohy, B. P. Tighe, and M. van Hecke, *Phys. Rev. E* **90**, 020202(R) (2014).
- [40] M. S. van Deen, B. P. Tighe, and M. van Hecke, *Phys. Rev. E* **94**, 062905 (2016).
- [41] C. Heussinger and J.-L. Barrat, *Phys. Rev. Lett.* **102**, 218303 (2009).
- [42] P. D’Haene, J. Mewis, and G. G. Fuller, *J. Colloid Interface Sci.* **156**, 350 (1993).